# Probing Two Driven Double Quantum Dots Strongly Coupled to a Cavity

Si-Si Gu,[1,2] Sigmund Kohler,[3,*] Yong-Qiang Xu,[1,2] Rui Wu,[1,2] Shun-Li Jiang,[1,2] Shu-Kun Ye,[1,2] Ting Lin,[1,2] Bao-Chuan Wang,[1,2] Hai-Ou Li,[1,2,4] Gang Cao,[1,2,4,†] and Guo-Ping Guo[1,2,4,5,‡]

[1]*CAS Key Laboratory of Quantum Information, University of Science and Technology of China, Hefei, Anhui 230026, China*
[2]*CAS Center for Excellence in Quantum Information and Quantum Physics, University of Science and Technology of China, Hefei, Anhui 230026, China*
[3]*Instituto de Ciencia de Materiales de Madrid, CSIC, E-28049 Madrid, Spain*
[4]*Hefei National Laboratory, University of Science and Technology of China, Hefei 230088, China*
[5]*Origin Quantum Computing Company Limited, Hefei, Anhui 230088, China*

(Received 20 December 2022; accepted 3 May 2023; published 9 June 2023)

We experimentally and theoretically study a driven hybrid circuit quantum electrodynamics (cQED) system beyond the dispersive coupling regime. Treating the cavity as part of the driven system, we develop a theory applicable to such strongly coupled and to multiqubit systems. The fringes measured for a single driven double quantum dot (DQD)-cavity setting and the enlarged splittings of the hybrid Floquet states in the presence of a second DQD are well reproduced with our model. This opens a path to study Floquet states of multiqubit systems with arbitrarily strong coupling and reveals a new perspective for understanding strongly driven hybrid systems.

DOI: 10.1103/PhysRevLett.130.233602

Semiconductor quantum dots (QDs) coupled to superconducting cavities provide a platform for investigating and exploiting light-matter interactions [1,2] with a potential for applications in solid-state quantum information processing. Since the coupling strength between the cavity and the qubits determines the speed of gate operations and information exchange [1–4], the development of circuit quantum electrodynamics (cQED) settings with strong interaction is of high interest. Experimental progress in QD-based cQED, such as high-impedance superconducting cavities [5,6], greatly increased the coupling strength, allowing systematic investigations of the physics of the Jaynes-Cummings model [6–13], the quantum Rabi model [14], and topology [15]. Moreover, it provides a direct path to integrate multiple qubits.

Strong periodic driving is a powerful and widely used tool in quantum control [16,17], quantum simulation [18,19], and system characterization [20–24]. Investigation of the corresponding Floquet dynamics is crucial for understanding such strongly driven systems [17] and provides a solid foundation for further improvements in practical applications [19,25,26]. Recently, Floquet spectroscopy [27] and the stationary Floquet state [28] of a driven double quantum dot (DQD) have been explored via a dispersively coupled cavity. Motivated by experimental advances, a theory for dispersive cavity readout of driven quantum systems has been proposed [29,30], restricted to settings with weak system-cavity coupling strengths within the linear-response limit. However, the weak coupling regime, which most of the experimental and theoretical works focused on, cannot meet the emerging need for large coupling strengths to perform coherent quantum information exchange and scalable quantum networks [2,4,31]. In addition, despite that a few works have studied two-DQD-cavity systems in the context of the Tavis-Cummings model and cavity-mediated long-range coupling between qubits [32–37], the dynamics of a driven multiqubit-cavity system remains unexplored.

In this Letter, we demonstrate a strongly driven hybrid system consisting of two spatially separated GaAs DQDs coupled to a superconducting NbTiN cavity. Benefiting from the enhanced coupling strength for the high-impedance cavity, the system is working beyond the scope of the existing theories for dispersive readout of strongly driven systems via a resonant cavity [27,29,30,38]. Different from these theories which treat the DQD as a relatively independent strongly driven system for the weak coupling strength, here we further develop a generalized theory by considering the Floquet states of the full hybrid system. In doing so, we treat the cavity as part of a central driven system, which provides an approach applicable for arbitrarily strong DQD-cavity coupling and also captures the cavity-mediated interaction between different DQDs. In our experiment, Landau-Zener-Stückelberg-Majorana (LZSM) interference patterns and splittings for a driven single DQD-cavity setup as well as the enlarged splittings for two-DQD-cavity system are experimentally observed in the cavity transmission. The results are analyzed and well reproduced with our model.

Figure 1(a) shows the half-wavelength superconducting NbTiN transmission cavity containing two DQDs ($\mathrm{DQD}_j$, $j = 1, 2$) separated by a distance of roughly 670 μm. Each DQD is connected to either voltage antinode of the

 

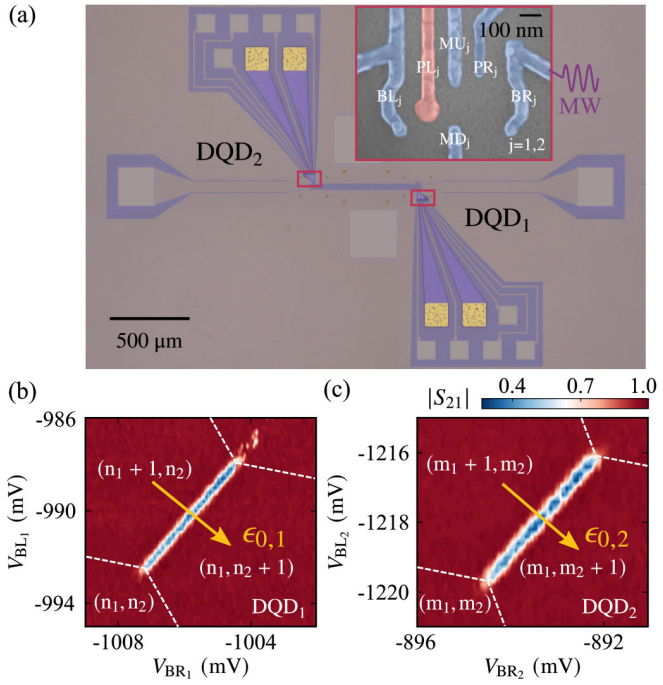


FIG. 1. (a) Optical micrograph of the device that is cooled to a temperature of ∼20 mK. Inset: false-color scanning electron micrograph of DQD$_j$ which can be tuned by the gate electrodes BL$_j$, PL$_j$, MU$_j$, PR$_j$, BR$_j$, and MD$_j$. The plunger gate PL$_j$ (red) is connected to the cavity. (b),(c) Charge stability diagrams of DQD$_1$ and DQD$_2$, respectively, as a function of gate voltages measured by the cavity transmission amplitude $|S_{21}|$, where $(n_1, n_2)$ and $(m_1, m_2)$ denote DQD occupations.

high-impedance ($Z_r \approx 2$ kΩ) cavity with a center frequency $\omega_c/2\pi = 5.196$ GHz and photon decay rate $\kappa/2\pi = 12.0$ MHz.

The DQDs are formed in a GaAs/AlGaAs quantum well with gate electrodes [inset in Fig. 1(a)]. The occupation numbers of the DQDs are controlled by gate voltages $V_{\mathrm{BR}_j}$ and $V_{\mathrm{BL}_j}$, as displayed in Figs. 1(b) and 1(c). An excess electron in DQD$_j$ forms a charge qubit described by the Hamiltonian,

$$H_{q,j} = \frac{\epsilon_j}{2}\sigma_{z,j} + t_j\sigma_{x,j}. \tag{1}$$

Here $\sigma$ denotes Pauli matrices, while $\epsilon_j$ is the energy detuning between the left and right dot of DQD$_j$, which can be adjusted by $V_{\mathrm{BR}_j}$. The interdot tunnel coupling $2t_j$ can be tuned via gate voltages $V_{\mathrm{MU}_j}$ and $V_{\mathrm{MD}_j}$.

The hybrid system is modeled by the Hamiltonian

$$H(t) = \sum_j H_{q,j}(t) + \sum_j \hbar g_j Z_j(a^\dagger + a) + \hbar\omega_c a^\dagger a, \tag{2}$$

where $a$ ($a^\dagger$) is the annihilation (creation) operator of a cavity photon, and $H_{q,j}(t)$ refers to DQD$_j$. Its scaled dipole operator $Z_j = \sigma_{z,j}$ couples to the electric field of the cavity with strength $g_j$. The coupling strength between DQD$_1$ and the cavity is estimated [39] to reach $g_1/2\pi = 85$ MHz at $2t_1/h \approx 5.2$ GHz with the DQD$_1$'s decoherence rate $\gamma_1/2\pi \approx 90$ MHz, while $g_2/2\pi = 80$ MHz at $2t_2/h \approx 5.16$ GHz with the decoherence rate $\gamma_2/2\pi \approx 100$ MHz for DQD$_2$. Experimentally, the continuous microwave is applied to gate BR$_j$ to periodically drive the system such that

$$\epsilon_j(t) = \epsilon_{0,j} + A_{d,j}\sin(2\pi f_d t) \tag{3}$$

with offset $\epsilon_{0,j}$, driving amplitude $A_{d,j}$, and driving frequency $f_d \equiv \Omega/2\pi$. We study the dynamics of the driven system by probing the transmission signal $|S_{21}|$ through the cavity.

To establish a theory for the transmission of a cavity coupled to various driven DQDs, one may extend the approach of Refs. [28–30,49] and consider the action of the cavity on each DQD and its backaction with nonequilibrium linear response theory. Since this approach is based on second-order perturbation theory in the weak DQD-cavity couplings, no cross terms between different DQDs occur, such that one can compute the impact of each DQD separately. Therefore, the shift of the cavity resonance, which governs the transmission, simply follows by summing the contributions of the individual DQDs.

Figure 2(a) visualizes this viewpoint for a single DQD. Within each driving period, the two relevant DQD states pick up a relative phase determined by the difference of the Floquet quasienergies. When it matches a multiple of $2\pi$, one observes fringes in the excitation probability [17]. The resonance condition for the cavity signal involves the cavity frequency and reads $\Delta\mu/\hbar = \omega_c + k\Omega$ with integer $k$ [30]. For a detailed discussion of these competing resonance conditions and their experimental verification, see Ref. [28].

The computed interference pattern for the parameters of our setup is shown in Fig. 2(b). Its fringes comply with the resonance condition, but for some values of the driving parameters the theory predicts transmissions up to 1.45 (red areas, marked by an arrow), which may indicate lasing [50–52]. Here, however, this is not the case. It is rather such that the DQD-cavity coupling strength is beyond the linear response limit, which leads to artefacts. Moreover, cavity-mediated interactions between the DQDs are ignored. Even when considering a realistic inhomogeneous broadening (see below), the computed transmission will still assume values up to 1.06. To overcome these shortcomings, we develop a theory for the readout of driven qubits in which the cavity is considered as part of the central system. Figure 2(c) illustrates this idea for a single DQD coupled to a cavity. This will allow us to treat settings with arbitrarily strong DQD-cavity coupling. For details of the derivation, see the Supplemental Material [39].

We start from the quantum Langevin equation for the cavity field $a$ with an inhomogeneity that corresponds to the Hamiltonian

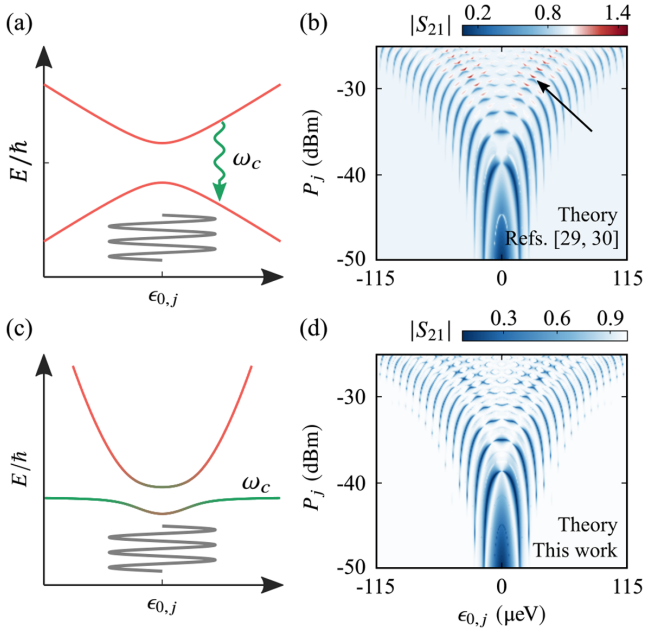


FIG. 2. (a) Schematic view of the approach of Refs. [29,30]. The system is formed by the energy levels of a single DQD (red) with sweeps induced by the microwave (gray). The cavity transmission is affected mainly when the DQD quasienergies match the cavity frequency. (b) Resulting transmission amplitude $|S_{21}|$. The black arrow marks out regions in which the transmission is larger than unity, which indicates that the DQD-cavity coupling exceeds the linear-response regime. (c) Theory of this Letter. The full DQD-cavity compound reacts to the excitation by the incoming fields. Red and green lines refer to the lowest DQD and cavity excitation energy, respectively. At the center (mixed color), the interaction hybridizes these states. (d) Corresponding transmission amplitude which obeys $|S_{21}| \leq 1$. The data are computed for microwave power $P_j = -40$ dBm which corresponds to the driving amplitude $A_{d,j} = 20.2$ μeV. The other parameters are $2t_j/\hbar = 5.2$ GHz, $g_j/2\pi = 85$ MHz, $f_d = 1.4$ GHz.

$$H_1(t) = -i\hbar \sum_{\nu=1,2} \sqrt{\kappa_\nu}\, a^\dagger a_{\mathrm{in},\nu}(t) + \mathrm{H.c.} \tag{4}$$

with the incoming fields $a_{\mathrm{in},\nu}$ and the cavity loss rate $\kappa_\nu$ at port $\nu = 1, 2$. The corresponding time-reversed equation relates incoming and outgoing fields as $a_{\mathrm{out},\nu} - a_{\mathrm{in},\nu} = \sqrt{\kappa_\nu} a$ [3,53]. Thus, to obtain the transmission, we have to compute how the $a_{\mathrm{in},\nu}$ affect the cavity operator $a$.

To this end, we employ nonequilibrium linear response theory for the perturbation caused by $H_1$. Since the cavity is probed at or close to resonance, $\omega_p \approx \omega_c$, the Hermitian conjugate contribution is off-resonant and, thus, can be neglected, such that the inputs act only via the cavity operator $a^\dagger$. In agreement with the Kubo formula, we find that the perturbation $a_{\mathrm{in},\nu}(t)$ and the response $\langle a(t)\rangle$ are linked by the susceptibility [39]

$$\chi(t,t') = -i\langle [a(t), a^\dagger(t')]\rangle_0 \theta(t-t'), \tag{5}$$

with the Heaviside step function $\theta$. Notice that here the expectation value $\langle\cdots\rangle_0$ considers the driven dissipative dynamics of the full DQDs-cavity compound. Since the DQDs are driven, the response depends explicitly on both times. Then $\langle a(t)\rangle$ is no longer given by a simple convolution, but acquires a summation over Fourier components $\chi^{(k)}(\omega)$. Nevertheless, for the experimentally relevant time-averaged cavity signal, knowledge of the component with $k = 0$ is sufficient [29,30,39]. Taking this average, the response in frequency space reads $\langle a_\omega\rangle = -i\sum_\nu \sqrt{\kappa_\nu}\chi^{(0)}(\omega) a_{\mathrm{in},\nu}(\omega)$. For an input at port $\nu = 1$ only, the input-output relation directly provides the time-averaged cavity transmission

$$S_{21}(\omega) = -i\sqrt{\kappa_1\kappa_2}\chi^{(0)}(\omega) \tag{6}$$

and the reflection $S_{11}(\omega) = 1 - i\kappa_1\chi^{(0)}(\omega)$.

The remaining task is the computation of $\chi^{(0)}(\omega)$ for which we proceed as in Refs. [28–30], but with the DQD Hamiltonian replaced by the full DQDs-cavity Hamiltonian (2). Following that scheme, we first compute the Floquet states $|\phi_\alpha(t)\rangle$ of $H(t)$ and the quasienergies $\mu_\alpha$ by solving the eigenvalue equation $[H(t) - i\hbar d/dt]|\phi(t)\rangle = \mu|\phi(t)\rangle$. The result is then used to evaluate the dissipative kernel of the Bloch-Redfield equation, which yields the transition rates between Floquet states and, hence, the steady-state populations of the Floquet states, $p_\alpha$. With these ingredients, the susceptibility in Eq. (6) becomes [39]

$$\chi^{(0)}(\omega) = \sum_{\alpha,\beta,k} \frac{(p_\alpha - p_\beta)|a_{\alpha\beta,k}|^2}{\omega + (\mu_\alpha - \mu_\beta)/\hbar - k\Omega + i\kappa/2}, \tag{7}$$

where $a_{\alpha\beta,k}$ is the $k$th Fourier component of the transition matrix element $a(t) = \langle\phi_\alpha(t)|a|\phi_\beta(t)\rangle$. The total cavity decay rate $\kappa = \kappa_1 + \kappa_2 + \kappa_{\mathrm{int}}$ consists of contributions from each port $\kappa_\nu$ and the internal losses $\kappa_{\mathrm{int}}$.

The corresponding theory prediction for a single DQD is shown in Fig. 2(d). In contrast to the theory of Refs. [29,30] [Fig. 2(b)], it obeys $|S_{21}| \leq 1$ in the whole range considered, which underlines the applicability of our theory for values of $g_j$ beyond the linear-response regime.

To demonstrate that the preceding theory enables a quantitative understanding of measurement results, firstly, $\mathrm{DQD}_1$ is driven and coupled to the cavity, while $\mathrm{DQD}_2$ is far detuned, $\epsilon_{0,2} \gg \hbar\omega_c$, and hence is inactive. Figure 3(a) shows the measured $|S_{21}|$ as a function of detuning $\epsilon_{0,1}$ and driving power $P_1 \propto A_{d,1}^2$, which maps out a LZSM interference pattern. Within the $|\epsilon_{0,1}| < A_{d,1}$ region, a series of interference fringes with amplitude minima significantly below unity are observed. When the states of the $\mathrm{DQD}_1$-cavity system interfere constructively, the excited Floquet state is effectively populated, resulting in a minima value of the numerator in Eq. (7) and a reduction in $|S_{21}|$. Figure 3(b) displays the theoretical result after convolution with a Gaussian that

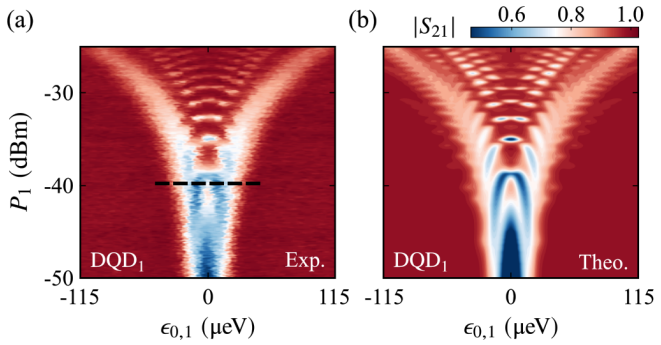


FIG. 3. (a) Measured transmission $|S_{21}|$ as a function of detuning $\epsilon_{0,1}$ and driving power $P_1$ for $DQD_1$ at $2t_1/h \approx 5.2$ with $f_d = 1.4$ GHz. (b) Corresponding theoretical result. The inhomogeneous broadening is considered by a convolution with a Gaussian of width $\sigma_\epsilon = 4$ μeV along the $\epsilon_{0,1}$ axis and $\sigma_P = 0.1$ dB along the $P_1$ axis [22,28,54].

captures the inhomogeneous broadening [22,28,54]. It is in very good agreement with the experimental data. Likewise, an equivalent experiment is carried out for the case of $DQD_2$ coupled with the cavity. The result is consistent with Fig. 3 and is shown in the Supplemental Material [39].

Scalable quantum information processing requires multiple qubits that interact with a cavity. As a reference, Fig. 4(a) shows the resulting measured $|S_{21}|$ for the $DQD_1$-cavity system as a function of the cavity probe frequency $\omega_p/2\pi$ and the detuning $\epsilon_{0,1}$. The drive power is fixed at $P_{d,1} = -39.9$ dBm, which is marked by a black dashed line in Fig. 3(a). The red bar with $|S_{12}| \approx 1$ is observed when the cavity is probed at resonances, $\omega_p = \omega_c$. In the spectral picture, this corresponds to an excitation energy $\hbar\omega_c$ sketched by the green line in the inset of Fig. 4(a). When the cavity frequency comes close to resonance with the DQD, the cavity and the DQD are hybridized, illustrated by the line color in the inset of Fig. 4(a). Then the driving leads to interference which induces a redistribution of DQD-cavity Floquet states, which is visible as gaps in the red bar with maximal transmission around $\epsilon_{0,1} = 0$ marked by yellow arrows. The corresponding data for $DQD_2$ is shown in Fig. S1 of the Supplemental Material [39].

We now turn to the case of a driven two-DQD-cavity hybrid system by tuning both DQDs close to resonance with the cavity and applying to both microwaves with the same frequency $f_d = 1.4$ GHz at gates $BR_1$ and $BR_2$. By simultaneously changing the detunings $\epsilon_{0,1}$ and $\epsilon_{0,2}$, we measure the transmission $|S_{21}|$ depicted in Fig. 4(b). Notably in comparison with the single DQD case [Fig. 4(a)], the gaps in the red bar become significantly larger.

In contrast to the single-DQD-cavity system, the two-DQD-cavity system is a multilevel system whose eigenenergies are schematically illustrated in the inset of Fig. 4(b). Nevertheless, the Floquet states acquire different phases during the driving period and interfere similarly,

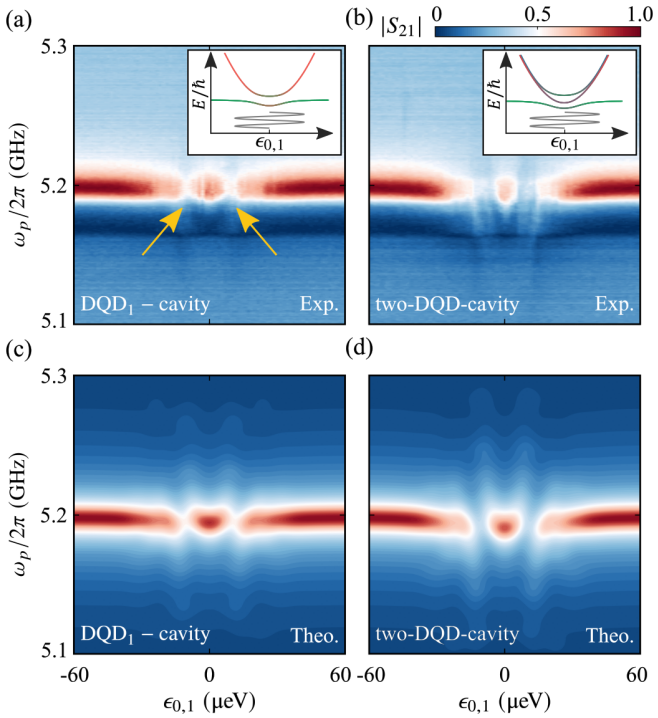


FIG. 4. Transmission $|S_{21}|$ as a function of probe frequency $\omega_p/2\pi$ and detuning $\epsilon_{0,1}$ for (a) the $DQD_1$-cavity system and (b) the two-DQD-cavity system. In (b), $\epsilon_{0,2}$ is simultaneously varied in the range of $(-68.3, 68.3)$ μeV, while $P_1 = -39.9$ and $P_2 = -42$ dBm are fixed. Insets: the energy level schematic diagram of the hybrid system. Red, blue, and green colors refer to the states $|e\rangle_1|g\rangle_2|0\rangle$, $|g\rangle_1|e\rangle_2|0\rangle$, $|g\rangle_1|g\rangle_2|1\rangle$, respectively, where $|g\rangle_j$ and $|e\rangle_j$ denote the ground and excited state of $DQD_j$ and $|n\rangle$ the $n$-photon cavity state. (c),(d) Theoretical results with the inhomogeneous broadening used in Fig. 3.

resulting in a change in the population distribution and a more pronounced impact on $|S_{21}|$. As is indicated by Eq. (7), besides the population, also $|a_{\alpha\beta,k}|^2$ and $\omega_p + (\mu_\alpha - \mu_\beta)/\hbar - k\Omega$ play a role in the signal. The increased hybridization of cavity photon with two DQDs leads to a decrease in $|a_{\alpha\beta,k}|^2$ and a larger deviation of the energy splitting $(\mu_\beta - \mu_\alpha)/\hbar + k\Omega$ from $\omega_p$. Therefore, enlarged splittings are observed. All the experimental features are well reproduced by the theoretical results in Figs. 4(c) and 4(d), which underlines that our approach is general and scalable.

In conclusion, we have investigated both experimentally and theoretically the driven dynamics of the hybrid system in which two DQDs are strongly coupled to a cavity. For the theoretical description, we have developed a method for the cavity transmission in which the cavity is considered as part of a Floquet system. This extends the method of Ref. [29] to cases with DQD-cavity coupling beyond the linear-response limit. Moreover, it allows one to treat multiple qubits that interact via the cavity. On a quantitative level, we have demonstrated the excellent agreement of

computed and measured LZSM patterns in a regime in which limitations of the former approach become visible. Our approach is applicable to cQED architecture built of other physical systems, such as QDs in other host materials and superconducting qubits. Our results provide a more profound insight into the dynamics of Floquet states and may motivate future applications in scalable hybrid quantum systems.

This work was supported by the National Natural Science Foundation of China (Grants No. 61922074, No. 92265113, No. 12074368, and No. 12034018), by the Innovation Program for Quantum Science and Technology (Grant No. 2021ZD0302300), by the Spanish Ministry of Science, Innovation, and Universities (Grant No. PID2020–117787 GB-I00), and by the CSIC Research Platform on Quantum Technologies PTI-001. This work was partially carried out at the USTC Center for Micro- and Nanoscale Research and Fabrication.

*sigmund.kohler@csic.es
†gcao@ustc.edu.cn
‡gpguo@ustc.edu.cn

[1] X. Gu, A. F. Kockum, A. Miranowicz, Y.-x. Liu, and F. Nori, Microwave photonics with superconducting quantum circuits, Phys. Rep. **718–719**, 1 (2017).
[2] G. Burkard, M. J. Gullans, X. Mi, and J. R. Petta, Superconductor-semiconductor hybrid-circuit quantum electrodynamics, Nat. Rev. Phys. **2**, 129 (2020).
[3] A. Blais, R.-S. Huang, A. Wallraff, S. M. Girvin, and R. J. Schoelkopf, Cavity quantum electrodynamics for superconducting electrical circuits: An architecture for quantum computation, Phys. Rev. A **69**, 062320 (2004).
[4] A. Blais, A. L. Grimsmo, S. M. Girvin, and A. Wallraff, Circuit quantum electrodynamics, Rev. Mod. Phys. **93**, 025005 (2021).
[5] N. Samkharadze, A. Bruno, P. Scarlino, G. Zheng, D. P. DiVincenzo, L. DiCarlo, and L. M. K. Vandersypen, High-Kinetic-Inductance Superconducting Nanowire Resonators for Circuit QED in a Magnetic Field, Phys. Rev. Appl. **5**, 044004 (2016).
[6] A. Stockklauser, P. Scarlino, J. V. Koski, S. Gasparinetti, C. K. Andersen, C. Reichl, W. Wegscheider, T. Ihn, K. Ensslin, and A. Wallraff, Strong Coupling Cavity QED with Gate-Defined Double Quantum Dots Enabled by a High Impedance Resonator, Phys. Rev. X **7**, 011030 (2017).
[7] J. J. Viennot, M. C. Dartiailh, A. Cottet, and T. Kontos, Coherent coupling of a single spin to microwave cavity photons, Science **349**, 408 (2015).
[8] X. Mi, J. V. Cady, D. M. Zajac, P. W. Deelman, and J. R. Petta, Strong coupling of a single electron in silicon to a microwave photon, Science **355**, 156 (2017).
[9] N. Samkharadze, G. Zheng, N. Kalhor, D. Brousse, A. Sammak, U. C. Mendes, A. Blais, G. Scappucci, and L. M. K. Vandersypen, Strong spin-photon coupling in silicon, Science **359**, 1123 (2018).
[10] A. J. Landig, J. V. Koski, P. Scarlino, U. C. Mendes, A. Blais, C. Reichl, W. Wegscheider, A. Wallraff, K. Ensslin, and T. Ihn, Coherent spin-photon coupling using a resonant exchange qubit, Nature (London) **560**, 179 (2018).
[11] X. Mi, M. Benito, S. Putz, D. M. Zajac, J. M. Taylor, G. Burkard, and J. R. Petta, A coherent spin-photon interface in silicon, Nature (London) **555**, 599 (2018).
[12] T. Bonsen, P. Harvey-Collard, M. Russ, J. Dijkema, A. Sammak, G. Scappucci, and L. M. K. Vandersypen, Probing the Jaynes-Cummings Ladder with Spin Circuit Quantum Electrodynamics, Phys. Rev. Lett. **130**, 137001 (2023).
[13] C. X. Yu, S. Zihlmann, J. C. Abadillo-Uriel, V. P. Michal, N. Rambal, H. Niebojewski, T. Bedecarrats, M. Vinet, E. Dumur, M. Filippone, B. Bertrand, S. De Franceschi, Y.-M. Niquet, and R. Maurand, Strong coupling between a photon and a hole spin in silicon, Nat. Nanotechnol. 10.1038/s41565-023-01332-3 (2023).
[14] P. Scarlino, J. H. Ungerer, D. J. van Woerkom, M. Mancini, P. Stano, C. Müller, A. J. Landig, J. V. Koski, C. Reichl, W. Wegscheider, T. Ihn, K. Ensslin, and A. Wallraff, In situ Tuning of the Electric-Dipole Strength of a Double-Dot Charge Qubit: Charge-Noise Protection and Ultrastrong Coupling, Phys. Rev. X **12**, 031004 (2022).
[15] B. Pérez-González, A. Gómez-León, and G. Platero, Topology detection in cavity QED, Phys. Chem. Chem. Phys. **24**, 15860 (2022).
[16] M. P. Silveri, J. A. Tuorila, E. V. Thuneberg, and G. S. Paraoanu, Quantum systems under frequency modulation, Rep. Prog. Phys. **80**, 056002 (2017).
[17] O. V. Ivakhnenko, S. N. Shevchenko, and F. Nori, Nonadiabatic Landau-Zener-Stückelberg-Majorana transitions, dynamics, and interference, Phys. Rep. **995**, 1 (2023).
[18] N. Goldman and J. Dalibard, Periodically Driven Quantum Systems: Effective Hamiltonians and Engineered Gauge Fields, Phys. Rev. X **4**, 031027 (2014).
[19] O. Kyriienko and A. S. Sørensen, Floquet Quantum Simulation with Superconducting Qubits, Phys. Rev. Appl. **9**, 064029 (2018).
[20] D. M. Berns, M. S. Rudner, S. O. Valenzuela, K. K. Berggren, W. D. Oliver, L. S. Levitov, and T. P. Orlando, Amplitude spectroscopy of a solid-state artificial atom, Nature (London) **455**, 51 (2008).
[21] J. Stehlik, Y. Dovzhenko, J. R. Petta, J. R. Johansson, F. Nori, H. Lu, and A. C. Gossard, Landau-Zener-Stückelberg interferometry of a single electron charge qubit, Phys. Rev. B **86**, 121303(R) (2012).
[22] F. Forster, G. Petersen, S. Manus, P. Hänggi, D. Schuh, W. Wegscheider, S. Kohler, and S. Ludwig, Characterization of Qubit Dephasing by Landau-Zener-Stückelberg-Majorana Interferometry, Phys. Rev. Lett. **112**, 116803 (2014).
[23] M. F. Gonzalez-Zalba, S. N. Shevchenko, S. Barraud, J. R. Johansson, A. J. Ferguson, F. Nori, and A. C. Betz, Gate-sensing coherent charge oscillations in a silicon field-effect transistor, Nano Lett. **16**, 1614 (2016).
[24] A. Bogan, S. Studenikin, M. Korkusinski, L. Gaudreau, P. Zawadzki, A. S. Sachrajda, L. Tracy, J. Reno, and T. Hargett, Landau-Zener-Stückelberg-Majorana Interferometry of a Single Hole, Phys. Rev. Lett. **120**, 207701 (2018).
[25] P. S. Mundada, A. Gyenis, Z. Huang, J. Koch, and A. A. Houck, Floquet-Engineered Enhancement of Coherence Times in a Driven Fluxonium Qubit, Phys. Rev. Appl. **14**, 054033 (2020).

[26] M. S. Rudner and N. H. Lindner, Band structure engineering and non-equilibrium dynamics in Floquet topological insulators, Nat. Rev. Phys. **2**, 229 (2020).
[27] J. V. Koski, A. J. Landig, A. Pályi, P. Scarlino, C. Reichl, W. Wegscheider, G. Burkard, A. Wallraff, K. Ensslin, and T. Ihn, Floquet Spectroscopy of a Strongly Driven Quantum Dot Charge Qubit with a Microwave Resonator, Phys. Rev. Lett. **121**, 043603 (2018).
[28] M.-B. Chen, B.-C. Wang, S. Kohler, Y. Kang, T. Lin, S.-S. Gu, H.-O. Li, G.-C. Guo, X. Hu, H.-W. Jiang, G. Cao, and G.-P. Guo, Floquet state depletion in ac-driven circuit QED, Phys. Rev. B **103**, 205428 (2021).
[29] S. Kohler, Dispersive Readout of Adiabatic Phases, Phys. Rev. Lett. **119**, 196802 (2017).
[30] S. Kohler, Dispersive readout: Universal theory beyond the rotating-wave approximation, Phys. Rev. A **98**, 023849 (2018).
[31] H. J. Kimble, The quantum internet, Nature (London) **453**, 1023 (2008).
[32] D. J. van Woerkom, P. Scarlino, J. H. Ungerer, C. Müller, J. V. Koski, A. J. Landig, C. Reichl, W. Wegscheider, T. Ihn, K. Ensslin, and A. Wallraff, Microwave Photon-Mediated Interactions between Semiconductor Qubits, Phys. Rev. X **8**, 041018 (2018).
[33] P. Scarlino, D. J. van Woerkom, U. C. Mendes, J. V. Koski, A. J. Landig, C. K. Andersen, S. Gasparinetti, C. Reichl, W. Wegscheider, K. Ensslin, T. Ihn, A. Blais, and A. Wallraff, Coherent microwave-photon-mediated coupling between a semiconductor and a superconducting qubit, Nat. Commun. **10**, 3011 (2019).
[34] A. J. Landig, J. V. Koski, P. Scarlino, C. Müller, J. C. Abadillo-Uriel, B. Kratochwil, C. Reichl, W. Wegscheider, S. N. Coppersmith, M. Friesen, A. Wallraff, T. Ihn, and K. Ensslin, Virtual-photon-mediated spin-qubit-transmon coupling, Nat. Commun. **10**, 5037 (2019).
[35] F. Borjans, X. G. Croot, X. Mi, M. J. Gullans, and J. R. Petta, Resonant microwave-mediated interactions between distant electron spins, Nature (London) **577**, 195 (2020).
[36] B. Wang, T. Lin, H. Li, S. Gu, M. Chen, G. Guo, H. Jiang, X. Hu, G. Cao, and G. Guo, Correlated spectrum of distant semiconductor qubits coupled by microwave photons, Sci. Bull. **66**, 332 (2021).
[37] P. Harvey-Collard, J. Dijkema, G. Zheng, A. Sammak, G. Scappucci, and L. M. K. Vandersypen, Coherent Spin-Spin Coupling Mediated by Virtual Microwave Photons, Phys. Rev. X **12**, 021026 (2022).
[38] S. N. Shevchenko, A. I. Ryzhov, and F. Nori, Low-frequency spectroscopy for quantum multilevel systems, Phys. Rev. B **98**, 195434 (2018).
[39] See Supplemental Material at http://link.aps.org/supplemental/10.1103/PhysRevLett.130.233602, which includes Refs. [40–48], for additional data and a detailed derivation of the formalism.
[40] K. D. Petersson, L. W. McFaul, M. D. Schroer, M. Jung, J. M. Taylor, A. A. Houck, and J. R. Petta, Circuit quantum electrodynamics with a spin qubit, Nature (London) **490**, 380 (2012).
[41] T. Frey, P. J. Leek, M. Beck, A. Blais, T. Ihn, K. Ensslin, and A. Wallraff, Dipole Coupling of a Double Quantum Dot to a Microwave Resonator, Phys. Rev. Lett. **108**, 046807 (2012).
[42] A. G. Redfield, On the theory of relaxation processes, IBM J. Res. Dev. **1**, 19 (1957).
[43] K. Blum, *Density Matrix Theory and Applications*, 2nd ed. (Springer, New York, 1996).
[44] A. J. Leggett, S. Chakravarty, A. T. Dorsey, M. P. A. Fisher, A. Garg, and W. Zwerger, Dynamics of the dissipative two-state system, Rev. Mod. Phys. **59**, 1 (1987).
[45] P. Hänggi, P. Talkner, and M. Borkovec, Reaction-rate theory: Fifty years after Kramers, Rev. Mod. Phys. **62**, 251 (1990).
[46] U. Weiss, *Quantum Dissipative Systems*, 2nd ed. (World Scientific, Singapore, 1998).
[47] J. Leppäkangas, J. D. Brehm, P. Yang, L. Guo, M. Marthaler, A. V. Ustinov, and M. Weides, Resonance inversion in a superconducting cavity coupled to artificial atoms and a microwave background, Phys. Rev. A **99**, 063804 (2019).
[48] C. W. Gardiner and P. Zoller, *Quantum Noise*, 3rd ed. (Springer, Berlin, 2004).
[49] X. Mi, S. Kohler, and J. R. Petta, Landau-Zener interferometry of valley-orbit states in Si/SiGe double quantum dots, Phys. Rev. B **98**, 161404(R) (2018).
[50] M. Marthaler, Y. Utsumi, and D. S. Golubev, Lasing in circuit quantum electrodynamics with strong noise, Phys. Rev. B **91**, 184515 (2015).
[51] Y.-Y. Liu, J. Stehlik, C. Eichler, M. J. Gullans, J. M. Taylor, and J. R. Petta, Semiconductor double quantum dot micromaser, Science **347**, 285 (2015).
[52] P. Neilinger, S. N. Shevchenko, J. Bogár, M. Rehák, G. Oelsner, D. S. Karpov, U. Hübner, O. Astafiev, M. Grajcar, and E. Il'ichev, Landau-Zener-Stückelberg-Majorana lasing in circuit quantum electrodynamics, Phys. Rev. B **94**, 094519 (2016).
[53] M. J. Collett and C. W. Gardiner, Squeezing of intracavity and traveling-wave light fields produced in parametric amplification, Phys. Rev. A **30**, 1386 (1984).
[54] J. Stehlik, Y.-Y. Liu, C. Eichler, T. R. Hartke, X. Mi, M. J. Gullans, J. M. Taylor, and J. R. Petta, Double Quantum Dot Floquet Gain Medium, Phys. Rev. X **6**, 041027 (2016).